

ARTICLE

Received 31 Mar 2015 | Accepted 3 Jul 2015 | Published 7 Aug 2015

DOI: 10.1038/ncomms8992

OPEN

# Molecular metal- $N_x$ centres in porous carbon for electrocatalytic hydrogen evolution

Hai-Wei Liang<sup>1</sup>, Sebastian Brüller<sup>1</sup>, Renhao Dong<sup>1,2</sup>, Jian Zhang<sup>2</sup>, Xinliang Feng<sup>2</sup> & Klaus Müllen<sup>1</sup>

Replacement of precious platinum with efficient and low-cost catalysts for electrocatalytic hydrogen evolution at low overpotentials holds tremendous promise for clean energy devices. Here we report a novel type of robust cobalt-nitrogen/carbon catalyst for the hydrogen evolution reaction (HER) that is prepared by the pyrolysis of cobalt- $N_4$  macrocycles or cobalt/*o*-phenylenediamine composites and using silica colloids as a hard template. We identify the well-dispersed molecular  $CoN_x$  sites on the carbon support as the active sites responsible for the HER. The  $CoN_x/C$  catalyst exhibits extremely high turnover frequencies per cobalt site in acids, for example, 0.39 and  $6.5\text{ s}^{-1}$  at an overpotential of 100 and 200 mV, respectively, which are higher than those reported for other scalable non-precious metal HER catalysts. Our results suggest the great promise of developing new families of non-precious metal HER catalysts based on the controlled conversion of homogeneous metal complexes into solid-state carbon catalysts via economically scalable protocols.

<sup>1</sup>Max-Planck-Institute for Polymer Research, Ackermannweg 10, 55128 Mainz, Germany. <sup>2</sup>Department of Chemistry and Food Chemistry & Center for Advancing Electronics Dresden (cfaed), Technische Universität Dresden, Mommsenstrasse 4, 01062 Dresden, Germany. Correspondence and requests for materials should be addressed to X.F. (email: xinliang.feng@tu-dresden.de) or to K.M. (email: muellen@mpip-mainz.mpg.de).

To meet the scientific challenges of the increasing global demand for energy and diminishing sources of fossil fuels, great efforts have been devoted to exploit alternative and renewable energy sources and carriers. The clean and efficient production of hydrogen through electrocatalytic processes, such as photoelectrochemical water splitting or electrolysis coupled to renewable energy sources, represents a promising and appealing solution as a next-generation technology for sustainable energy conversion<sup>1–3</sup>. The development of active hydrogen evolution reaction (HER) electrocatalysts with low overpotentials is crucial for the successful implementation of water splitting technologies. Although platinum-based catalysts have proven as the most efficient electrocatalysts for HER, the prohibitive cost and scarcity of platinum significantly hinder its widespread technological use. It is thus highly desirable to develop low-cost catalyst systems based on earth-abundant elements that are capable of producing hydrogen from water with high catalytic activity and stability<sup>4–10</sup>.

Inspired by the naturally occurring hydrogen evolution and uptake on hydrogenase enzymes, chemists have made great breakthroughs in recent years on the development of bioinspired, synthetic metal complex HER catalysts, including cobaloxime<sup>7,11</sup>, cobalt diimine–dioxime<sup>12</sup> and nickel phosphane compounds<sup>13</sup>, which are molecularly similar to the Fe–Fe and Fe–Ni active sites of hydrogenases. Unfortunately, most bioinspired catalysts suffer from instability in aqueous solution and require large overpotentials to achieve appreciable turnover frequencies (TOFs).<sup>12–15</sup> The practical utilization of these synthetic molecular catalysts in aqueous electrolytes therefore requires their careful grafting onto carbon nanotubes by additional and complex chemical processes<sup>14,15</sup>. In contrast, independent efforts in solid-state electrocatalysis have led to several efficient inorganic crystalline catalysts, such as transition metal dichalcogenides<sup>16–24</sup>, phosphides<sup>25–27</sup>, carbides<sup>28–31</sup>, nitrides<sup>32,33</sup>, borides<sup>28</sup> and metallic nanoparticles embedded in carbon.<sup>34,35</sup> Despite their promising performance, it is highly challenging to control the atomic-scale surface structure of these inorganic materials and to preferentially expose a greater fraction of their active sites, for example, the edge sites of transition metal dichalcogenides<sup>21,23</sup>.

In this study, we demonstrate an up-scalable, solid-state, carbon-based catalyst for HER with molecular CoN<sub>x</sub> active sites that are structurally similar to molecular metal–N<sub>4</sub> macrocycle catalysts. The CoN<sub>x</sub>/C catalysts are prepared by a straightforward pyrolysis process at high temperature in which cobalt–N<sub>4</sub> macrocycles or cobalt/*o*-phenylenediamine composites are used as precursors and silica colloid is used as template. The achieved catalysts exhibit a high specific surface area (1,074 m<sup>2</sup> g<sup>−1</sup>) and well-dispersed, highly active CoN<sub>x</sub> active sites. In strong acid electrolytes (for example, 0.5 M H<sub>2</sub>SO<sub>4</sub>), the CoN<sub>x</sub>/C catalyst shows an overpotential of only 133 mV at a current density of 10 mA cm<sup>−2</sup>. Moreover, acid leaching and thiocyanate ion poisoning experiments identify that the well-dispersed molecular CoN<sub>x</sub> centres in carbon are responsible for the outstanding HER performance of the CoN<sub>x</sub>/C catalysts. Importantly, the CoN<sub>x</sub>/C catalysts exhibit unprecedented TOFs (TOFs per Co atom of 0.39 and 6.5 s<sup>−1</sup> at an overpotential of 100 and 200 mV, respectively), which are superior to those of the recently reported breakthrough HER catalysts based on biomimetic molecules<sup>14,15</sup>, metal dichalcogenides<sup>18,21</sup> and phosphides<sup>25–27</sup> (TOF < 1.0 s<sup>−1</sup> at 200 mV overpotential).

## Results

**Electrocatalyst preparation.** A schematic diagram describing the catalyst preparation is shown in Fig. 1. Three different precursors were examined in this work for the construction of the CoN<sub>x</sub>/C catalysts, including metal–N<sub>4</sub> macrocycles, that is, cobalt tetramethoxyphenylporphyrin (CoTMPP) and vitamin V12 (VB12),

as well as the cobalt/*o*-phenylenediamine composites (Co-*o*PD). To improve the porosity of the carbon-based catalysts, silica nanoparticles were used as hard template during the synthesis<sup>36,37</sup>. Typically, a mixture of C/N/Co precursors and silica colloids (HS40, 12 nm) was first subjected to pyrolysis at different temperatures in the range of 600–1,000 °C under N<sub>2</sub> atmosphere. The pyrolyzed product was then etched in a 2.0 M NaOH solution to remove the silica template. The NaOH-treated sample was next treated in 0.5 M H<sub>2</sub>SO<sub>4</sub> at 90 °C for 4 h to leach out unstable, metallic cobalt nanoparticles. Two additional heat treatments at the same temperature as for the pyrolysis step were carried out after the NaOH and H<sub>2</sub>SO<sub>4</sub> etching. During the pyrolysis of the metal complex, the precursors decomposed and formed carbon-based materials integrated with active CoN<sub>x</sub> moieties. The pyrolysis temperature was optimized for each precursor according to its HER activity (Supplementary Fig. 1). We found that the Co-*o*PD catalyst pyrolyzed at 900 °C yielded the highest HER activity (Supplementary Fig. 2). Therefore, the CoN<sub>x</sub>/C catalysts discussed below were all produced from Co-*o*PD at 900 °C unless otherwise specified. For comparison, metal-free N/C, nitrogen-free Co/C and pure carbon catalysts were also prepared (details of the fabrication process for all materials are given in the Methods section).

**Electrocatalytic performance for HER.** The HER performance of the CoN<sub>x</sub>/C catalysts and reference samples, including N/C, Co/C and a commercially available Pt/C (20 wt% Pt, BASF), was first evaluated using the rotating disk electrode (RDE) technique in an Ar-saturated 0.5 M H<sub>2</sub>SO<sub>4</sub> solution. As shown in Fig. 2a, metal-free nitrogen-doped carbon (N/C) can act as a HER catalyst, although the overpotential is quite high (460 mV at 10 mA cm<sup>−2</sup>). According to previous reports, nitrogen doping could reduce the Gibbs free energy of hydrogen adsorption and result in an improved HER activity compared with pure carbon materials<sup>38</sup>. The Co/C catalyst exhibited higher HER activity than the metal-free N/C catalyst and the pure carbon material (Supplementary Fig. 3); it had an overpotential of 310 mV at a current density of 10 mA cm<sup>−2</sup>, which is comparable to those of the Fe/Co nanoparticle-based catalysts that were recently reported<sup>34,35</sup>. The simultaneous incorporation of nitrogen and cobalt into carbon led to a profound enhancement of the HER activity, as reflected by the large shift of the polarization curve of the CoN<sub>x</sub>/C catalyst to a lower overpotential compared with the N/C and Co/C catalysts (Fig. 2a). In particular, the CoN<sub>x</sub>/C catalyst showed an overpotential of only 133 and 156 mV at a current density of 10 and 20 mA cm<sup>−2</sup> (after ohmic and capacitive corrections, see Supplementary Fig. 4 for details), respectively, which are only ~100 mV lower than the benchmark Pt/C catalyst (overpotential of 32 mV at 10 mA cm<sup>−2</sup>). Moreover, the overpotential of the CoN<sub>x</sub>/C catalyst is much lower than the values reported for most acid-stable, earth-abundant, molecular and inorganic HER electrocatalysts (Supplementary Table 1), including CNTs-supported nickel bisdiphosphine complexes (300 mV overpotential at 4 mA cm<sup>−2</sup>)<sup>14</sup> and cobalt diimine–dioxime complexes (590 mV overpotential at 1 mA cm<sup>−2</sup>)<sup>15</sup>, electrodeposited H<sub>2</sub>-CoCat catalysts (385 mV overpotential at 2 mA cm<sup>−2</sup>)<sup>39</sup>, ordered double-gyroid MoS<sub>2</sub> bicontinuous networks, and chemically exfoliated WS<sub>2</sub> nanosheets (~240 mV overpotential at 10 mA cm<sup>−2</sup> for the latter two cases)<sup>21,23</sup>. In addition, the overpotential reached by the CoN<sub>x</sub>/C catalysts is comparable to those of highly active metal phosphide and carbide nanoparticle catalysts (70–130 mV overpotential at 10 mA cm<sup>−2</sup>)<sup>25,27</sup>.

The electrochemical impedance spectroscopy (EIS) analysis also confirmed a faster HER kinetic process on CoN<sub>x</sub>/C than on

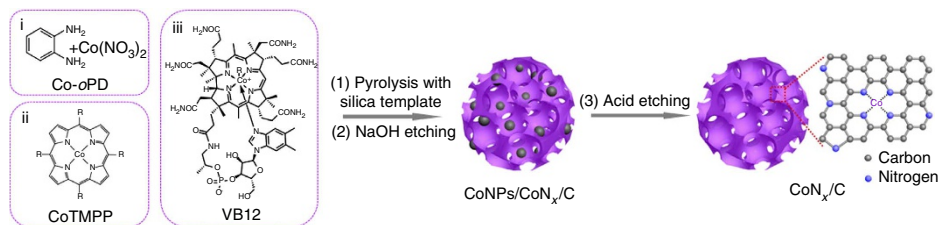


**Figure 1 | Schematic illustration of the synthesis of the  $\text{CoN}_x/\text{C}$  electrocatalysts.** (1) Mixing of carbon, nitrogen, and cobalt precursors (Co-oPD, CoTMPP, or VB12) with the silica template and pyrolyzing of the mixture; (2) NaOH etching to remove the silica template and form  $\text{CoNPs}/\text{CoN}_x/\text{C}$  composites; (3) Acid etching with  $\text{H}_2\text{SO}_4$  to remove Co-containing nanoparticles and formation of carbon-based catalysts containing  $\text{CoN}_x$  sites. The second and third heat treatments after the NaOH and  $\text{H}_2\text{SO}_4$  etching steps are not shown.

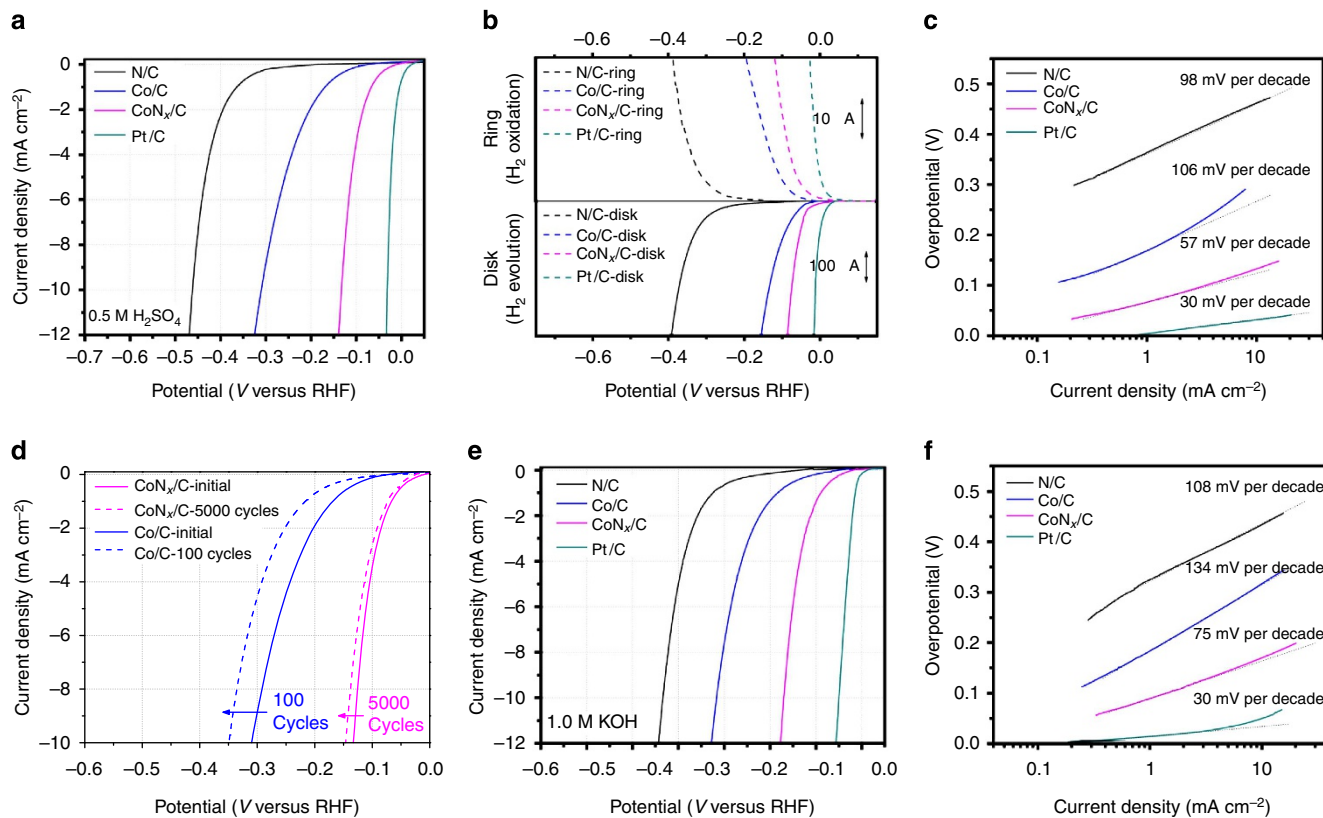


**Figure 2 | Electrocatalytic performance of the  $\text{CoN}_x/\text{C}$  electrocatalysts.** (a) HER polarization plots of the  $\text{CoN}_x/\text{C}$ , N/C, Co/N and Pt/C catalysts in 0.5 M  $\text{H}_2\text{SO}_4$ . (b) RRDE measurements of hydrogen evolution from a 0.5 M  $\text{H}_2\text{SO}_4$  solution on different catalyst-modified electrodes. The Pt-ring electrode was maintained at 0.7 V for the oxidation of the  $\text{H}_2$  that was evolved on the disk electrode. (c) Tafel plots obtained from the polarization curves in a. (d) Initial and post-potential cyclic voltammograms of  $\text{CoN}_x/\text{C}$  (5000 cycles) and Co/N (100 cycles) in 0.5 M  $\text{H}_2\text{SO}_4$ . Potential sweeps were cycled between 0.2 and  $-0.25$  V versus RHE (not iR-corrected). (e) HER polarization plots of  $\text{CoN}_x/\text{C}$ , N/C, Co/N and Pt/C catalysts in 1.0 M KOH. (f) Tafel plots obtained from the polarization curves in e. For all RDE and RRDE measurements, the catalyst loading is  $2.0 \text{ mg cm}^{-2}$  for non-Pt materials and  $0.2 \text{ mg cm}^{-2}$  ( $40 \mu\text{g}_{\text{Pt}} \text{ cm}^{-2}$ ) for the Pt/C catalyst. For  $\text{CoN}_x/\text{C}$  catalysts, the cobalt loading is only  $2.8 \mu\text{g}_{\text{Co}} \text{ cm}^{-2}$ , based on the ICP-AES measurements. Electrode rotation speed: 1,600 r.p.m.; scan rate:  $5 \text{ mVs}^{-1}$ .

N/C and Co/C (Supplementary Fig. 5). Furthermore, we found that the HER activity of  $\text{CoN}_x/\text{C}$  continuously increased with the cobalt/oPD ratio (up to  $\sim 10$  wt%) in the precursor materials (Supplementary Fig. 6). Further increasing the cobalt/oPD ratio to 20 wt% caused a dramatic decrease in activity, primarily due to the seriously reduced porosity of the carbon-based catalysts. The strong correlation between the HER activity and the amount of metal in the 0–10 wt% range probably indicates that the cobalt species are directly related to the active sites (see below for more details of the discussion).

The evolution of hydrogen on different catalysts was confirmed by the rotating ring disk electrode (RRDE) technique<sup>14</sup>. The disk electrode bearing the catalyst was rotated at 1,600 r.p.m. to

remove any  $\text{H}_2$  produced on the disk radially. Simultaneously, the Pt ring that encircles the disk electrode was maintained at 0.7 V versus reversible hydrogen electrode (RHE) to oxidize the  $\text{H}_2$  and produce a ring current. The selective detection of  $\text{H}_2$  formation by RRDE confirmed that all the catalysts generated  $\text{H}_2$  within the defined potentials (Fig. 2b). In particular, the electrocatalytic hydrogen evolution on the  $\text{CoN}_x/\text{C}$ -modified electrode occurred with an overpotential of only 20 mV (Fig. 2b), much lower than that observed on N/C- ( $\sim 220$  mV) and Co/C- ( $\sim 60$  mV) modified electrodes.

Figure 2c displays the Tafel plots of the polarization curves that provide insight into the HER pathways on various catalysts. The Pt/C-modified electrode exhibited a Tafel slope of  $\sim 30$  mV per

decade, which is consistent with the known mechanism of HER on Pt. The N/C and Co/C catalysts showed a Tafel slope of  $\sim 98$  and  $\sim 106$  mV per decade, respectively, suggesting that an initial proton adsorption was the rate-determining step on these two catalysts<sup>40</sup>. The Tafel analysis of the CoN<sub>x</sub>/C catalyst revealed a Tafel slope of  $\sim 57$  mV per decade, which may suggest hydrogen production via the Volmer–Heyrovsky mechanism, and that the electrochemical desorption step is rate limiting<sup>40</sup>. On the basis of the Tafel analysis, the exchange current density of the CoN<sub>x</sub>/C catalyst was estimated to be  $\sim 7 \times 10^{-5}$  A cm<sup>-2</sup>. This value is much higher than that reported for the electrodeposited H<sub>2</sub>-CoCat catalyst ( $\sim 3.2 \times 10^{-6}$  A cm<sup>-2</sup>)<sup>39</sup>, CNTs-supported nickel bisdiphosphine complex ( $\sim 3.2 \times 10^{-7}$  A cm<sup>-2</sup>)<sup>14</sup>, and C<sub>3</sub>N<sub>4</sub>/N-doped graphene ( $3.5 \times 10^{-7}$  A cm<sup>-2</sup>)<sup>41</sup>.

Electrochemical stability is an important requirement for a HER catalyst. An accelerated degradation study<sup>25,42</sup> was therefore carried out to assess the stability of the CoN<sub>x</sub>/C catalyst in 0.5 M H<sub>2</sub>SO<sub>4</sub>. For comparison, the Co/C catalyst was also examined under the same condition. Although the Co/C catalyst showed a moderate activity at the beginning, the HER performance rapidly decreased with the potential cycling (Fig. 2d). After 100 cyclic voltammetry (CV) cycles, the overpotential required to achieve a current density of 10 mA cm<sup>-2</sup> on the Co/C catalyst increased by  $> 40$  mV. The rapid degradation of the Co/C catalyst is likely associated with the gradual leaching out of cobalt species during the electrochemical process in the strong acid electrolyte. In sharp contrast, even after 5,000 CV cycles, only a slight negative shift of the HER polarization of the CoN<sub>x</sub>/C catalyst (11 mV shift of the overpotential at 10 mA cm<sup>-2</sup>) was observed, which suggests the superior durability of CoN<sub>x</sub>/C for HER.

Encouraged by the high electrochemical stability of the CoN<sub>x</sub>/C catalyst, we further studied the HER performance in alkaline and neutral media. The CoN<sub>x</sub>/C system catalysed the HER much more efficiently than did the N/C and Co/C catalysts in both the alkaline and neutral media, exhibiting an overpotential of 170 and 247 mV at a current density of 10 mA cm<sup>-2</sup> in 1.0 M KOH and 1.0 M phosphate buffer solutions (pH 7), respectively (Fig. 2e and Supplementary Fig. 7). These overpotentials compare favourably with the values reported for most non-precious metal HER catalysts under similar conditions (Supplementary Table 2), such as cobalt nanoparticle-based catalysts<sup>34,43</sup>, tungsten carbonitride<sup>31</sup> and copper molybdenum sulfide<sup>44</sup>. The CoN<sub>x</sub>/C catalyst showed a Tafel slope of  $\sim 75$  mV per decade in alkaline medium, which is much lower than those of N/C and Co/C catalysts (Fig. 2f). Moreover, the CoN<sub>x</sub>/C catalyst also exhibited negligible degradation in both alkaline and neutral media (Supplementary Fig. 8). The ability to operate over a wide range of pH makes the CoN<sub>x</sub>/C catalyst very flexible to coupling with favourable anodic catalysts for different types of water splitting devices<sup>1,45</sup>.

**Physical characterization of the CoN<sub>x</sub>/C catalysts.** To gain insights into the origin of the superior catalytic activity of the CoN<sub>x</sub>/C catalyst, different physical characterizations were conducted. Transmission electron microscopy (TEM) observations revealed that the CoNPs/CoN<sub>x</sub>/C catalyst prepared without acid leaching consisted of mesoporous carbon frameworks dispersed with irregular inorganic particles (Fig. 3a) that were identified as metallic cobalt by X-ray diffraction analysis (Supplementary Fig. 9). Upon leaching with acid, all cobalt nanoparticles were removed, as indicated by the TEM image and X-ray diffraction patterns (Fig. 3b and Supplementary Fig. 9, 10) of the CoN<sub>x</sub>/C catalyst. The absence of cobalt nanoparticles in the CoN<sub>x</sub>/C catalyst was further confirmed by magnetic measurement (Supplementary Fig. 11). N<sub>2</sub> sorption tests were performed to

evaluate the porous properties of the catalysts (Supplementary Figs 12, 13 and Supplementary Table 3). The steep and high capillary condensation steps in the isotherms revealed a uniform and well-developed mesoporosity with a large mesopore volume, which is in good agreement with the TEM observations. The considerable adsorption at the low relative pressure indicated the microporosity as well. Notably, the acid leaching resulted in a considerable increase in the apparent Brunauer–Emmett–Teller (BET) surface area from 745 m<sup>2</sup> g<sup>-1</sup> for CoNPs/CoN<sub>x</sub>/C to 1,074 m<sup>2</sup> g<sup>-1</sup> for CoN<sub>x</sub>/C without deterioration of the mesoporosity.

The high-resolution TEM image disclosed that the CoN<sub>x</sub>/C catalyst is composed of randomly orientated graphene layers without any metal particle or nanoscaled clusters (Fig. 3c). Importantly, elemental mapping with sub-nanoscale energy-filtered TEM (EFTEM) imaging revealed that both the nitrogen and the cobalt elements were homogeneously distributed throughout the whole carbon matrix (Fig. 3b). X-ray photoelectron spectroscopy (XPS) analysis was performed to probe the chemical composition of CoNPs/CoN<sub>x</sub>/C and CoN<sub>x</sub>/C. The surface nitrogen and cobalt contents of the CoNPs/CoN<sub>x</sub>/C catalyst were 3.3 ( $\pm 0.3$ ) and 1.2 ( $\pm 0.3$ ) at%, respectively (Fig. 3d and Supplementary Table 3). After acid leaching, the nitrogen content increased slightly to 3.9 ( $\pm 0.3$ ) at% for the CoN<sub>x</sub>/C catalyst, but no cobalt signal could be observed because of the relatively high detection limit ( $\sim 0.1$  at%) of the XPS technique (Fig. 3e). Inductively coupled plasma atomic emission spectrometry (ICP-AES) showed a bulk cobalt content of 0.14 ( $\pm 0.02$ ) wt% in the CoN<sub>x</sub>/C catalysts, significantly less than that of the CoNPs/CoN<sub>x</sub>/C catalyst (7.5  $\pm$  0.5 wt%). The high-resolution N1s spectrum suggested that the CoN<sub>x</sub>/C catalyst contained primarily pyridinic and graphitic nitrogen, together with a small amount of pyrrolic nitrogen and oxidized nitrogen species (Fig. 3f).

**Understanding the active sites.** The influence of the acid leaching of the CoN<sub>x</sub>/C catalyst on the HER activity was studied to determine whether the metallic cobalt nanoparticles contribute to the electrocatalytic HER. By comparing the HER polarization curves of the CoNPs/CoN<sub>x</sub>/C and CoN<sub>x</sub>/C catalysts, we found a sufficient improvement in HER activity after acid leaching (Fig. 4a). Such observation clearly excludes the contribution of metallic cobalt or cobalt oxide nanoparticles to the HER that was recently reported to be at least partly responsible for the catalytic hydrogen evolution<sup>34,35,39,46</sup>. In our catalyst system, acid leaching eliminated the inactive inorganic cobalt phase and exposed a larger carbon surface, which resulted in an increased BET surface area, as confirmed by the N<sub>2</sub> sorption tests (Supplementary Fig. 12), which in turn led to enhanced HER performance.

To further understand the nature of the active sites of the CoN<sub>x</sub>/C catalyst, we investigated the influence of thiocyanate ions (SCN<sup>-</sup>) on the HER activity of the CoN<sub>x</sub>/C, N/C and Co/N catalysts. SCN<sup>-</sup> is widely known to poison the metal-centred catalytic sites in acidic conditions<sup>47,48</sup>. On introducing SCN<sup>-</sup> into the acidic electrolyte (10 mM), the overpotential of the CoN<sub>x</sub>/C catalyst increased by  $> 35$  mV (Fig. 4b) and the current density significantly decreased from 16.2 to 6.2 mA cm<sup>-2</sup> at the overpotential of 150 mV (Supplementary Fig. 14), which suggests that  $> 60\%$  cobalt sites were blocked by the SCN<sup>-</sup> ions. Interestingly, no appreciable decrease of HER activity was observed for the N/C catalyst in the presence of SCN<sup>-</sup> ions (Supplementary Fig. 15), which indicated that there were no poisoning effects of SCN<sup>-</sup> on the metal-free nitrogen-doped carbon catalyst. Additionally, the SCN<sup>-</sup> ions also poisoned seriously the nitrogen-free Co/C catalyst (Supplementary Fig. 15),



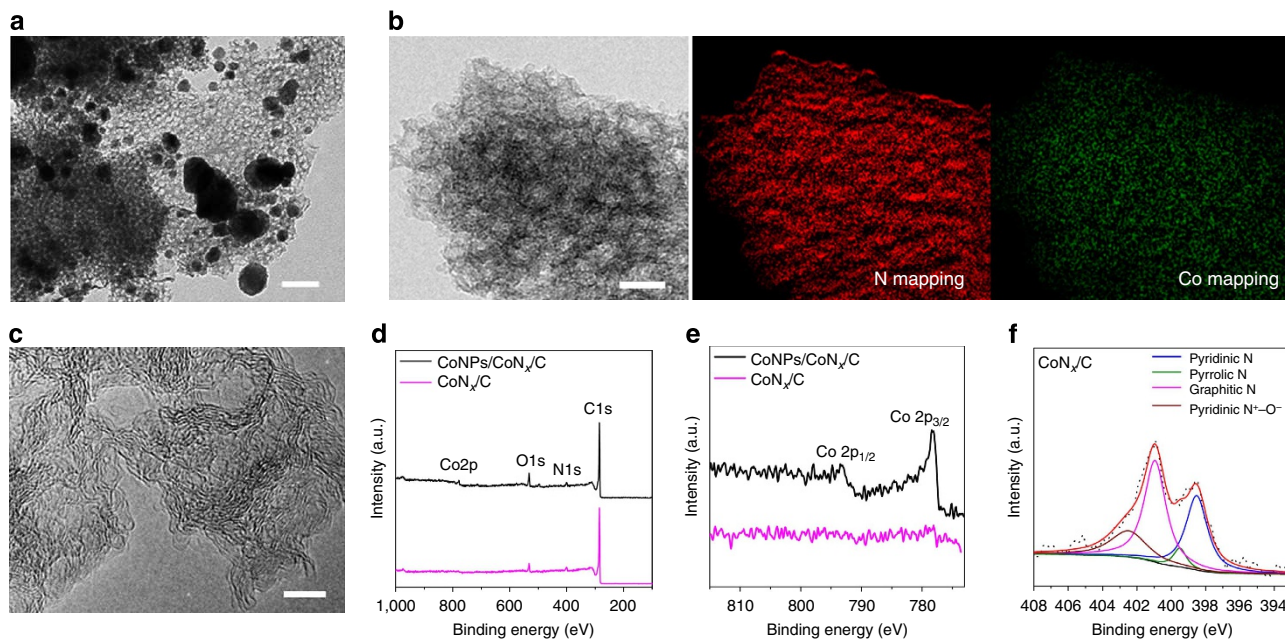


**Figure 3 | Catalyst characterization.** (a) TEM image of CoNPs/CoN<sub>x</sub>/C. Scale bar, 100 nm. (b) TEM image of CoN<sub>x</sub>/C and corresponding EFTEM elemental mapping demonstrating the homogeneous distribution of both cobalt and nitrogen at the atomic scale. Scale bar, 20 nm. (c) High-resolution TEM image of CoN<sub>x</sub>/C showing the layered graphene structure without any metal particles or nanoclusters. Scale bar, 5 nm. (d) XPS survey spectra of CoNPs/CoN<sub>x</sub>/C and CoN<sub>x</sub>/C. (e) High-resolution Co2p spectra of CoNPs/CoN<sub>x</sub>/C and CoN<sub>x</sub>/C. (f) High-resolution N1s spectra of CoN<sub>x</sub>/C.

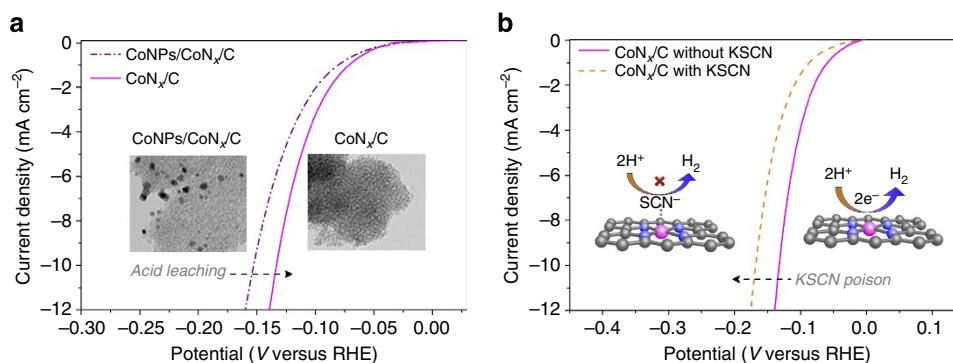


**Figure 4 | Understanding the structure of the active sites.** (a) Comparison of the HER activity of the CoNPs/CoN<sub>x</sub>/C and CoN<sub>x</sub>/C catalysts showing the influence of acid leaching. Insets are TEM images demonstrating that all cobalt particles were removed by acid leaching. (b) HER polarization plots of CoN<sub>x</sub>/C with and without 10 mM KSCN in 0.5 M H<sub>2</sub>SO<sub>4</sub>, indicating that SCN<sup>-</sup> ions strongly poison the CoN<sub>x</sub>/C catalyst. Insets are illustrations of cobalt centres blocked by the SCN<sup>-</sup> ions. These measurements indicated that the cobalt is involved in the active centers but not in the form of metallic nanoparticles.

although the cobalt-centred sites without nitrogen coordination were unstable in acidic conditions, as revealed by the accelerated degradation study (Fig. 2d). These results, combined with the EFTEM mapping as well as with XPS and high-resolution TEM analyses, strongly highlighted that after acid leaching, the surviving ionic cobalt species were well distributed in the carbon/nitrogen matrix and coordinated with nitrogen, at least partly, to form active and acid-resistant CoN<sub>x</sub> centres.

**TOF of the CoN<sub>x</sub>/C catalyst.** After assigning the active sites of the CoN<sub>x</sub>/C catalyst to the cobalt-containing centres, we estimated the TOF per cobalt site, which indicates the intrinsic per-site activity of a catalyst and is the best figure of merit for comparing activities among different catalysts. We determined the upper limit of the active sites to be  $\sim 2.85 \times 10^{16}$  sites per cm<sup>2</sup>, based on the hypothesis that all the cobalt atoms in the CoN<sub>x</sub>/C catalyst formed active CoN<sub>x</sub> centres and all of them were accessible to the electrolyte (details of the calculation are provided

in the Supplementary Information and Supplementary Note 1). Accordingly, the TOF values per cobalt site of the CoN<sub>x</sub>/C catalyst were calculated by this method and plotted against the applied overpotential, as shown in Fig. 5. In particular, the TOFs of CoN<sub>x</sub>/C are 0.39 H<sub>2</sub> per s and 6.5 H<sub>2</sub> per s at overpotentials of 100 and 200 mV, respectively. For the purpose of direct comparison, Fig. 5 also includes the TOF values of seven state-of-the-art non-precious metal HER catalysts published recently, including UHV-deposited MoS<sub>2</sub> nanoparticles supported on Au(111) (ref. 17), [Mo<sub>3</sub>S<sub>13</sub>]<sup>2-</sup> clusters on HOPG and graphite paper<sup>42</sup>, double-gyroid MoS<sub>2</sub> (ref. 21), Ni<sub>2</sub>P NPs (ref. 25), CoP NPs (ref. 27), Ni-bisdiphosphine molecular catalysts supported on CNTs (ref. 14), and electrodeposited H<sub>2</sub>-CoCat catalysts<sup>39</sup>. Clearly, the CoN<sub>x</sub>/C catalyst outperformed the recently reported scalable molecular or solid-state HER catalysts. The TOF values of CoN<sub>x</sub>/C are only slightly lower than those of UHV-deposited MoS<sub>2</sub> nanoparticles at overpotentials larger than 120 mV, although the latter could not be prepared via a scalable synthesis route<sup>17</sup>.

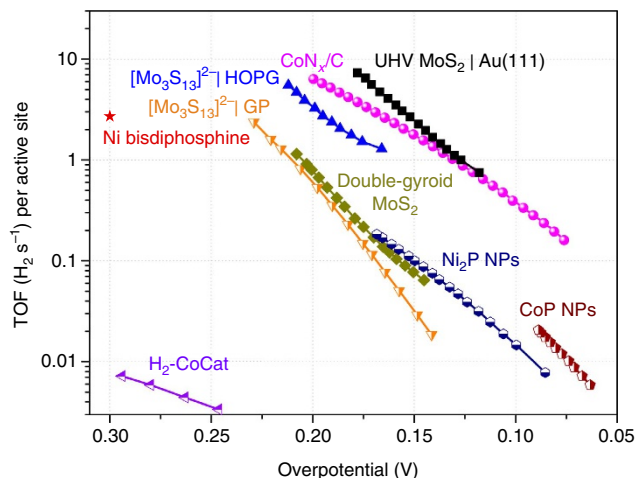


**Figure 5 | Comparison of the TOF of  $\text{CoN}_x/\text{C}$  with other catalysts.**

TOF plots of the  $\text{CoN}_x/\text{C}$  catalyst together with other recently reported molecular and inorganic HER catalysts. Data adapted from: ref. 17 for UHV  $\text{MoS}_2/\text{Au}$  (111); ref. 42 for  $[\text{Mo}_3\text{S}_{13}]^{2-}|\text{HOPG}$  and  $[\text{Mo}_3\text{S}_{13}]^{2-}|\text{graphite}$  paper; ref. 21 for double-gyroid  $\text{MoS}_2$ ; ref. 25 for  $\text{Ni}_2\text{P}$  NPs; ref. 27 for  $\text{CoP}$  NPs; ref. 14 for Ni-bisdiphosphine/CNTs; ref. 39 for  $\text{H}_2\text{-CoCat}$ . Data for  $\text{CoN}_x/\text{C}$  is from the present study.

## Discussion

To summarize, we demonstrated scalable, solid-state, carbon-based HER catalysts that contain molecular  $\text{CoN}_x$  active centres and exhibit an extremely high activity and excellent stability in aqueous solutions over a wide range of pH values. We attribute the outstanding HER performance of the  $\text{CoN}_x/\text{C}$  catalysts to the  $\text{CoN}_x$  centres generated during the pyrolysis of the metal- $\text{N}_4$  macrocycles or cobalt-*o*-phenylenediamine complexes, which are identified to be the active sites for HER by the acid leaching and thiocyanate ion poisoning experiments. The TOF values per cobalt site towards HER of our catalysts in an acidic electrolyte are substantially higher than those of reported non-precious metal molecular and solid-state HER catalysts. Further mechanistic studies are still required to unravel the exact structure of the active sites of the  $\text{CoN}_x/\text{C}$  catalyst and to better understand the involved reaction mechanism.

There is still a large room for the further improvement of the HER activity of  $\text{MeN}_x/\text{C}$  catalysts. Optimizing the Co-N binding properties or increasing the porosity by regulating the synthetic parameters (for example,  $\text{NH}_3$  post treatment<sup>37,49</sup>) would be an effective way to enhance the intrinsic activity per site as well as the HER performance on a geometric area basis. Further exploration of other  $\text{MeN}_x$  or bimetallic centres for HER would also provide many opportunities in this field, although we found that  $\text{CoN}_x$  was the best among several  $\text{MeN}_x/\text{C}$  catalysts (Supplementary Fig. 16). Moreover, bimetallic centres (for example,  $\text{CoNi-N}_x$ ,  $\text{CoMn-N}_x$ ) or even other coordinated atoms (for example, molecular  $\text{Me-S}_x$  (ref. 42) and  $\text{Me-P}_x$  (ref. 13) centres) could potentially lead to an enhancement in the catalytic activity for the HER and finally enable the catalysts to compete against the best Pt/C catalyst in technological devices. Considering the much lower metal content of the  $\text{CoN}_x/\text{C}$  catalyst than those of the recently reported metal nanoparticle-based catalysts<sup>34,35,43</sup>, future work will be also dedicated to increasing the density of  $\text{CoN}_x$  sites. The heterogeneous solid-state catalysts with molecular active sites described in the present work shed new light on the future development of earth-abundant catalysts for other important electrochemical processes, such as oxygen evolution, hydrogen oxidation and  $\text{CO}_2$  reduction.

## Methods

**Electrocatalyst synthesis.** Three different precursors have been used for the synthesis of the  $\text{CoN}_x/\text{C}$  catalysts, including a mixture of *o*PD and  $\text{Co}(\text{NO}_3)_2$ , CoTMPP and VB12 (Fig. 1). To prepare the  $\text{CoN}_x/\text{C}$  (Co-*o*PD) catalyst, 3.0 g *o*PD monomer was dissolved in 60 ml 1.0 M  $\text{HNO}_3$ ; then, 22.5 g silica colloid solution (Ludox HS40, ~12 nm, 40 wt%) and 1.5 g  $\text{Co}(\text{NO}_3)_2 \cdot 6\text{H}_2\text{O}$  were added. After stirring for ~10 min, the mixture was dried by using a rotary evaporator. The dried powder was pyrolyzed under flowing  $\text{N}_2$  for 2 h at temperatures ranging from 700 to 1,000 °C. Then, the silica template was etched out with 2.0 M NaOH. Subsequently, the sample was subjected to the second heat treatment in  $\text{N}_2$  atmosphere for 2 h to form the  $\text{CoNPs}/\text{CoN}_x/\text{C}$  composite. Finally, the catalyst was leached in 0.5 M  $\text{H}_2\text{SO}_4$  at 90 °C for 4 h to remove the cobalt-containing particles and was heat-treated again in  $\text{N}_2$  atmosphere for 2 h. All heat treatments were performed at the same temperature.

For comparison, a metal-free N-doped carbon catalyst (N/C) was prepared by the same process, although without adding  $\text{Co}(\text{NO}_3)_2 \cdot 6\text{H}_2\text{O}$ . The nitrogen-free Co-doped catalyst (Co/N) was prepared by the pyrolysis of a mixture containing 3.0 g sucrose, 15 g Ludox HS40 silica colloid (dry weight, 6.0 g), and 1.5 g  $\text{Co}(\text{NO}_3)_2 \cdot 6\text{H}_2\text{O}$ , followed by the same heat treatment and NaOH/ $\text{H}_2\text{SO}_4$  etching steps. A pure carbon catalyst was prepared by the same method although without adding  $\text{Co}(\text{NO}_3)_2 \cdot 6\text{H}_2\text{O}$ .

For the synthesis of the  $\text{CoN}_x/\text{C}$  (CoTMPP) catalyst, a mixture of 1.0 g CoTMPP and 1.0 g fumed silica (7 nm, Sigma-Aldrich S5130) was thoroughly ground in an agate mortar for at least 30 min. Then, the mixed powder was subjected to the heat treatment and NaOH/ $\text{H}_2\text{SO}_4$  etching steps. For the synthesis of the  $\text{CoN}_x/\text{C}$  (VB12) catalyst, 1.0 g VB12 was first dissolved in 50 ml distilled water, and 2.5 g silica colloid solution (Ludox HS40, ~12 nm, 40 wt%) was then added. After drying the solution with a rotary evaporator, the mixture underwent the same heat treatment and NaOH/ $\text{H}_2\text{SO}_4$  etching process, as described above.

For each  $\text{CoN}_x/\text{C}$  catalyst, the temperature of the heat treatment was optimized as a function of HER activity. The best temperature was found to be 900, 800 and 700 °C for the Co-*o*PD, CoTMPP and VB12-derived catalysts, respectively (Supplementary Fig. 1).

**Electrochemical measurements.** All electrochemical measurements were carried out in a conventional three-electrode cell using a WaveDriver 20 bipotentiostat (Pine Instrument Company, USA) controlled at room temperature. Ag/AgCl (4 M KCl) and platinum wire were used as reference and counter electrodes, respectively. All potentials in this study refer to those of the RHE. The potential difference between Ag/AgCl and RHE was determined based on the calibration measurement in  $\text{H}_2$ -saturated electrolyte. An RDE with a glassy carbon disk (5.0 mm diameter) and an RRDE with both a Pt ring (6.25 mm inner-diameter and 7.92 mm outer-diameter) and a glassy carbon disk (5.61 mm diameter) served as the substrate for the working electrodes in evaluating the HER activity and confirming the hydrogen evolutions. Before use, the glassy carbon electrodes in RDE/RRDE were polished using aqueous alumina suspensions on felt polishing pads. For the stability study, a graphite rod was used as the counter electrode to avoid the possible contribution of dissolved Pt species to the HER.

The catalyst ink was prepared by blending 10 mg of each catalyst with 100  $\mu\text{l}$  Nafion solution (0.5 wt%) and 0.4 ml ethanol in an ultrasonic bath. A certain volume of catalyst ink was then pipetted onto the glassy carbon surface to result in the desirable catalyst loading. The RDE/RRDE tests were measured in an Ar-saturated electrolyte at 1,600 r.p.m. with a sweep rate of  $5 \text{ mV s}^{-1}$ . The measured HER polarization curves were capacity corrected by taking an average of forward and backward (positive and negative-going) scans. For detecting the hydrogen evolved at the disc electrode, the potential of the Pt-ring electrode in the RRDE system was set to 0.7 V versus RHE. EIS spectra were recorded in an Ar-saturated electrolyte with a 5 mV AC potential from 10 kHz to 0.01 Hz at 1,600 r.p.m. For comparison, the commercial 20 wt% platinum on Vulcan carbon black catalyst (Pt/C from BASF) was measured under the same experimental conditions. The catalysts loading are  $2.0 \text{ mg cm}^{-2}$  for non-Pt materials and  $0.2 \text{ mg cm}^{-2}$  ( $40 \mu\text{g}_{\text{Pt}} \text{ cm}^{-2}$ ) for the Pt/C catalyst. For the  $\text{CoN}_x/\text{C}$  catalyst, the cobalt loading is only  $2.8 \mu\text{g}_{\text{Co}} \text{ cm}^{-2}$ , based on the ICP-AES measurements.

**Characterization.** TEM was performed using a JEM-1400 microscope (JEOL Ltd., Japan) operating at an accelerating voltage of 200 kV. High-resolution TEM measurements were conducted on a Tecnai F20 (FEI) microscope with a beam voltage of 200 kV. EFTEM mapping was performed using a JEM-ARM 200F microscope operating at an accelerating voltage of 200 kV. Elemental mapping were collected using a Gatan GIF Quantum 965. XPS experiments were carried out on an AXIS Ultra DLD system from Kratos with Al K $\alpha$  radiation. X-ray diffraction spectra were recorded on a PW1820 powder diffractometer (Phillips) using a Cu-K $\alpha$  emitter. Nitrogen sorption measurements were conducted at 77 K on a TriStar 3020 volumetric analyser (Micromeritics). All samples were degassed at 300 °C for at least 4 h before every measurement. Specific surface areas were determined by the standard BET method based on the relative pressure between 0.05 and 0.20. The pore size distribution was calculated using the non-local density functional theory method. ICP-AES measurements were conducted on an Atomscan Advantage Spectrometer (Thermo Ash Jarrell Corporation).

## References

- Walter, M. G. *et al.* Solar water splitting cells. *Chem. Rev.* **110**, 6446–6473 (2010).
- Lewis, N. S. & Nocera, D. G. Powering the planet: chemical challenges in solar energy utilization. *Proc. Natl Acad. Sci. USA* **103**, 15729–15735 (2006).
- Crabtree, G. W. & Dresselhaus, M. S. The hydrogen fuel alternative. *MRS Bull.* **33**, 421–428 (2008).
- Artero, V., Chavarot-Kerlidou, M. & Fontecave, M. Splitting water with cobalt. *Angew. Chem. Int. Ed.* **50**, 7238–7266 (2011).
- Merki, D. & Hu, X. Recent developments of molybdenum and tungsten sulfides as hydrogen evolution catalysts. *Energ. Environ. Sci.* **4**, 3878–3888 (2011).
- Laursen, A. B., Kegnaes, S., Dahl, S. & Chorkendorff, I. Molybdenum sulfides-efficient and viable materials for electro- and photoelectrocatalytic hydrogen evolution. *Energ. Environ. Sci.* **5**, 5577–5591 (2012).
- Dempsey, J. L., Brunschwig, B. S., Winkler, J. R. & Gray, H. B. Hydrogen evolution catalyzed by cobaloximes. *Acc. Chem. Res.* **42**, 1995–2004 (2009).
- Jiao, Y., Zheng, Y., Jaroniec, M. & Qiao, S. Z. Design of electrocatalysts for oxygen- and hydrogen-involving energy conversion reactions. *Chem. Soc. Rev.* **44**, 2060–2086 (2015).
- Zheng, Y., Jiao, Y., Jaroniec, M. & Qiao, S. Z. Advancing the electrochemistry of the hydrogen-evolution reaction through combining experiment and theory. *Angew. Chem. Int. Ed.* **54**, 52–65 (2015).
- Duan, J., Chen, S., Jaroniec, M. & Qiao, S. Z. Porous C<sub>3</sub>N<sub>4</sub> nanolayers@N-graphene films as catalyst electrodes for highly efficient hydrogen evolution. *ACS Nano* **9**, 931–940 (2015).
- Baffert, C., Artero, V. & Fontecave, M. Cobaloximes as functional models for hydrogenases. 2. Proton electroreduction catalyzed by difluoroborylbis(dimethylglyoximate)cobalt(II) complexes in organic media. *Inorg. Chem.* **46**, 1817–1824 (2007).
- Jacques, P.-A., Artero, V., Pécaut, J. & Fontecave, M. Cobalt and nickel diimine-dioxime complexes as molecular electrocatalysts for hydrogen evolution with low overvoltages. *Proc. Natl Acad. Sci. USA* **106**, 20627–20632 (2009).
- Helm, M. L., Stewart, M. P., Bullock, R. M., DuBois, M. R. & DuBois, D. L. A synthetic nickel electrocatalyst with a turnover frequency above 100,000 s<sup>-1</sup> for H<sub>2</sub> production. *Science* **333**, 863–866 (2011).
- Le Goff, A. *et al.* From hydrogenases to noble metal-free catalytic nanomaterials for H<sub>2</sub> production and uptake. *Science* **326**, 1384–1387 (2009).
- Andriadis, E. S. *et al.* Molecular engineering of a cobalt-based electrocatalytic nanomaterial for H<sub>2</sub> evolution under fully aqueous conditions. *Nat. Chem.* **5**, 48–53 (2013).
- Hinnemann, B. *et al.* Biomimetic hydrogen evolution: MoS<sub>2</sub> nanoparticles as catalyst for hydrogen evolution. *J. Am. Chem. Soc.* **127**, 5308–5309 (2005).
- Jaramillo, T. F. *et al.* Identification of active edge sites for electrochemical H<sub>2</sub> evolution from MoS<sub>2</sub> nanocatalysts. *Science* **317**, 100–102 (2007).
- Chen, Z. *et al.* Core-shell MoO<sub>3</sub>-MoS<sub>2</sub> nanowires for hydrogen evolution: a functional design for electrocatalytic materials. *Nano Lett.* **11**, 4168–4175 (2011).
- Li, Y. G. *et al.* MoS<sub>2</sub> nanoparticles grown on graphene: an advanced catalyst for the hydrogen evolution reaction. *J. Am. Chem. Soc.* **133**, 7296–7299 (2011).
- Merki, D., Fierro, S., Vrubel, H. & Hu, X. L. Amorphous molybdenum sulfide films as catalysts for electrochemical hydrogen production in water. *Chem. Sci.* **2**, 1262–1267 (2011).
- Kibsgaard, J., Chen, Z., Reinecke, B. N. & Jaramillo, T. F. Engineering the surface structure of MoS<sub>2</sub> to preferentially expose active edge sites for electrocatalysis. *Nat. Mater.* **11**, 963–969 (2012).
- Lukowski, M. A. *et al.* Enhanced hydrogen evolution catalysis from chemically exfoliated metallic MoS<sub>2</sub> nanosheets. *J. Am. Chem. Soc.* **135**, 10274–10277 (2013).
- Voiry, D. *et al.* Enhanced catalytic activity in strained chemically exfoliated WS<sub>2</sub> nanosheets for hydrogen evolution. *Nat. Mater.* **12**, 850–855 (2013).
- Gao, M.-R. *et al.* An efficient molybdenum disulfide/cobalt diselenide hybrid catalyst for electrochemical hydrogen generation. *Nat. Commun.* **6**, 5982 (2015).
- Popczun, E. J. *et al.* Nanostructured nickel phosphide as an electrocatalyst for the hydrogen evolution reaction. *J. Am. Chem. Soc.* **135**, 9267–9270 (2013).
- Kibsgaard, J. & Jaramillo, T. F. Molybdenum phosphosulfide: an active, acid-stable, earth-abundant catalyst for the hydrogen evolution reaction. *Angew. Chem. Int. Ed.* **53**, 14433–14437 (2014).
- Popczun, E. J., Read, C. G., Roske, C. W., Lewis, N. S. & Schaak, R. E. Highly active electrocatalysis of the hydrogen evolution reaction by cobalt phosphide nanoparticles. *Angew. Chem. Int. Ed.* **53**, 5427–5430 (2014).
- Vrubel, H. & Hu, X. Molybdenum boride and carbide catalyze hydrogen evolution in both acidic and basic solutions. *Angew. Chem. Int. Ed.* **51**, 12703–12706 (2012).
- Chen, W. F. *et al.* Highly active and durable nanostructured molybdenum carbide electrocatalysts for hydrogen production. *Energ. Environ. Sci.* **6**, 943–951 (2013).
- Liao, L. *et al.* A nanoporous molybdenum carbide nanowire as an electrocatalyst for hydrogen evolution reaction. *Energ. Environ. Sci.* **7**, 387–392 (2014).
- Zhao, Y., Kamiya, K., Hashimoto, K. & Nakanishi, S. Hydrogen evolution by tungsten carbonitride nanoelectrocatalysts synthesized by the formation of a tungsten acid/polymer hybrid *in situ*. *Angew. Chem. Int. Ed.* **52**, 13638–13641 (2013).
- Chen, W.-F. *et al.* Hydrogen-evolution catalysts based on non-noble metal nickel-molybdenum nitride nanosheets. *Angew. Chem. Int. Ed.* **51**, 6131–6135 (2012).
- Cao, B., Veith, G. M., Neuefeind, J. C., Adzic, R. R. & Khalifah, P. G. Mixed close-packed cobalt molybdenum nitrides as non-noble metal electrocatalysts for the hydrogen evolution reaction. *J. Am. Chem. Soc.* **135**, 19186–19192 (2013).
- Zou, X. *et al.* Cobalt-embedded nitrogen-rich carbon nanotubes efficiently catalyze hydrogen evolution reaction at all pH values. *Angew. Chem. Int. Ed.* **53**, 4372–4376 (2014).
- Deng, J. *et al.* Highly active and durable non-precious-metal catalyst encapsulated in carbon nanotubes for hydrogen evolution reaction. *Energ. Environ. Sci.* **7**, 1919–1923 (2014).
- Yang, W., Feller, T.-P. & Antonietti, M. Efficient metal-free oxygen reduction in alkaline medium on high-surface-area mesoporous nitrogen-doped carbons made from ionic liquids and nucleobases. *J. Am. Chem. Soc.* **133**, 206–209 (2010).
- Liang, H.-W., Zhuang, X., Brüller, S., Feng, X. & Müllen, K. Hierarchically porous carbons with optimized nitrogen doping as highly active electrocatalysts for oxygen reduction. *Nat. Commun.* **5**, 4973 (2014).
- Zheng, Y. *et al.* Toward design of synergistically active carbon-based catalysts for electrocatalytic hydrogen evolution. *ACS Nano* **8**, 5290–5296 (2014).
- Cobo, S. *et al.* A Janus cobalt-based catalytic material for electro-splitting of water. *Nat. Mater.* **11**, 802–807 (2012).
- Conway, B. E. & Tilak, B. V. Interfacial processes involving electrocatalytic evolution and oxidation of H<sub>2</sub>, and the role of chemisorbed H. *Electrochim. Acta* **47**, 3571–3594 (2002).
- Zheng, Y. *et al.* Hydrogen evolution by a metal-free electrocatalyst. *Nat. Commun.* **5**, 3783 (2014).
- Kibsgaard, J., Jaramillo, T. F. & Besenbacher, F. Building an appropriate active-site motif into a hydrogen-evolution catalyst with thiomolybdate [Mo<sub>3</sub>S<sub>13</sub>]<sup>2-</sup> clusters. *Nat. Chem.* **6**, 248–253 (2014).
- Wang, J. *et al.* Cobalt nanoparticles encapsulated in nitrogen-doped carbon as a bifunctional catalyst for water electrolysis. *J. Mater. Chem. A* **2**, 20067–20074 (2014).
- Tran, P. D. *et al.* Copper molybdenum sulfide: a new efficient electrocatalyst for hydrogen production from water. *Energ. Environ. Sci.* **5**, 8912–8916 (2012).
- Reece, S. Y. *et al.* Wireless solar water splitting using silicon-based semiconductors and earth-abundant catalysts. *Science* **334**, 645–648 (2011).
- Tavakkoli, M. *et al.* Single-shell carbon-encapsulated iron nanoparticles: synthesis and high electrocatalytic activity for hydrogen evolution reaction. *Angew. Chem. Int. Ed.* **54**, 4535–4538 (2015).
- Thorum, M. S., Hankett, J. M. & Gewirth, A. A. Poisoning the oxygen reduction reaction on carbon-supported Fe and Cu electrocatalysts: evidence for metal-centered activity. *J. Phys. Chem. Lett.* **2**, 295–298 (2011).
- Wang, Q. *et al.* Phenylendiamine-based FeN<sub>x</sub>/C catalyst with high activity for oxygen reduction in acid medium and its active-site probing. *J. Am. Chem. Soc.* **136**, 10882–10885 (2014).
- Proietti, E. *et al.* Iron-based cathode catalyst with enhanced power density in polymer electrolyte membrane fuel cells. *Nat. Commun.* **2**, 416 (2011).

## Acknowledgements

This work was financially supported by the ERC Grant on NANOGRAPH and 2DMATER, EU Project GENIUS and MoQuas, EC under Graphene Flagship (No. CNECT-ICT-604391) and MaxNet Energy. We thank Sergii I. Shylin for assistance with the magnetic measurement.

## Author contributions

K.M., X.F. and H.W.L. conceived and designed the experiments. H.W.L. conducted the synthesis of the catalysts. H.W.L., S.B. and J.Z. performed the electrochemical measurements. R.D. performed the TEM measurements. H.W.L., X.F. and K.M. co-wrote the paper. All authors discussed the results and commented on the manuscript.

## Additional information

**Supplementary Information** accompanies this paper at <http://www.nature.com/naturecommunications>

**Competing financial interests:** The authors declare no competing financial interests.



**Reprints and permission** information is available online at <http://npg.nature.com/reprintsandpermissions/>

**How to cite this article:** Liang, H.-W. *et al.* Molecular metal–N<sub>x</sub> centres in porous carbon for electrocatalytic hydrogen evolution. *Nat. Commun.* 6:7992 doi: 10.1038/ncomms8992 (2015).



This work is licensed under a Creative Commons Attribution 4.0 International License. The images or other third party material in this article are included in the article's Creative Commons license, unless indicated otherwise in the credit line; if the material is not included under the Creative Commons license, users will need to obtain permission from the license holder to reproduce the material. To view a copy of this license, visit <http://creativecommons.org/licenses/by/4.0/>